

TonB-Dependent Receptors Activity Reduction Strategy in *Xanthomonas oryzae* pv. *oryzae* Pathogenicity: A Computational Approach

Dharmendra Kashyap^{1,2*}, Amita Shakya¹ and DSVGK Kaladhar², Leena Preeti Lakra³

¹Amity Institute of Biotechnology, Amity University Chhattisgarh, Raipur, Pin 493225

²Dept of Microbiology and Bioinformatics, U.T.D. of Atal Bihari Vajpayee Vishwavidyalaya, Bilaspur, Chhattisgarh, Pin 495009

³Dept of Food Processing and Technology, U.T.D. of Atal Bihari Vajpayee Vishwavidyalaya, Bilaspur, Chhattisgarh Pin 495009

***Corresponding Author: Dharmendra Kashyap**
*Email: dharmendra.kashyap@bilaspuruniversity.ac.in

ABSTRACT

Introduction: Rice, a vital staple crop globally, feeding over 3.5 billion people and providing about 20% of global caloric intake. In India, cultivated on 44 million hectares, contributing 20-25% to GDP and employing over 50% of the workforce. *Xanthomonas oryzae* pv. *oryzae* (Xoo) is a Gram-negative bacterium responsible for bacterial blight (BB), one of the most devastating diseases of Rice crop, worldwide. Xoo enters rice leaves through hydathodes or wounds, multiplies in the xylem, and spreads systemically, leading to leaf wilting, reduced photosynthesis, and significant yield losses, particularly in Asia and parts of Africa. The pathogenicity of Xoo relies on a suite of virulence factors, including the type III secretion system (T3SS) for effector delivery, extracellular polysaccharides, cell wall-degrading enzymes, cell membrane associated transport proteins. The aim is to study cell membrane associated transport proteins responsible for secretion using computational tools and screen come best performing compounds from Zinc15 database to mitigate their efficiency.

Materials and Methods: The study includes sequences of *Xanthomonas oryzae* pv. *oryzae* PXO99A, virulence factors identification using advanced machine learning tools like (SVMs, HMMs), three dimensional structure modelling using AlphaFold2 server, energy-minimization using YASARA, and validation using most efficient online tools i.e. ModFOLD, ERRAT, VERIFY3D, VADAR, PROCHECK, Draggability and ligand-binding sites mapping with CavityPlus server, CavPharmer tool and Virtual screening and docking of over 80,000 ZINC15 ligands (Secondary metabolites) through MTiOpenScreen and DockThor tool and Molecular interaction analysis with Swiss Dock-Vina and ADMET properties analysis using Artificial Intelligence driven tools of S.M.University's AI Drug Lab.

Results and Discussion: Computational analysis of ACD59730.1 TonB-dependent outer membrane Receptor and ACD60174.1 TonB-dependent Receptor/Oar-like protein done using AlphaFold2 for 3D structure prediction. Both the proteins showed higher model quality with both structures validated as stable and accurate predicted by YASARA, ModFOLD, ERRAT, VERIFY3D, VADAR, and PROCHECK.

Conclusion: A small group of ligands were identified by docking studies from a vast dataset with good potential as inhibitors to these proteins, which can be used to mitigate the infection of Xoo. The study provides a thorough understanding in membrane associated proteins in Xoo's pathogenicity and identifying potential therapeutic targets through advanced computational tools.

KEYWORDS: *Xanthomonas oryzae* pv. *oryzae*, Rice (*Oryza sativa* L.), TonB-dependent membrane Receptors, Bacterial Leaf Blight, ZINC15 database.

How to Cite: Dharmendra Kashyap, Amita Shakya and DSVGK Kaladhar, Leena Preeti Lakra., (2025) TonB-Dependent Receptors Activity Reduction Strategy in *Xanthomonas oryzae* pv. *oryzae* Pathogenicity: A Computational Approach, Vascular and Endovascular Review, Vol.8, No.13s, 50-63.

INTRODUCTION

Xanthomonas oryzae pv. *oryzae* (Xoo) is a Gram's-negative bacterium responsible for bacterial blight (BB), one of the most destructive diseases of rice (*Oryza sativa* L.) worldwide. Xoo enters rice leaves through hydathodes or wounds, multiplies in the xylem, and spreads using xylum and phloem, leading to leaf wilting, reduced photosynthesis, and significant yield losses, particularly in semi-tropical regions of Asia and parts of Africa (Niño-Liu et al., 2006). The pathogenicity of Xoo relies on a suite of virulence factors, including the type I to VI secretion system for effector delivery, extracellular polysaccharides secretion, cell wall-degrading enzymes, and nutrient acquisition systems adapted to the nutrient-poor xylem environment. Xoo enters rice leaves via hydathodes or wounds, colonizes the xylem, and relies on an array of virulence factors, including the hypersensitive response and pathogenicity encoded by various secretion system (T3SS), extracellular polysaccharides, and nutrient acquisition systems specifically tailored to the iron- and carbohydrate-limited xylem environment (Choi et al., 2020).

Among these, TonB-dependent membrane receptors (TBDRs, also known as TonB-dependent transporters or TBDRs) play a notable role in active transport of molecules across the outer membrane. TBDRs are β -barrel proteins powered by the TonB-ExbB-ExbD complex, which harnesses the proton motive force from the inner membrane to drive uptake of scarce, high-molecular-weight substrates such as iron-siderophore complexes, vitamin B12, and, in phytopathogens, plant-derived carbohydrates (Blanvillain et al., 2007; Noinaj et al., 2010). In *Xanthomonas* species, genomes encode an unusually high number of TBDRs (up to 70–100), reflecting adaptation to plant-associated niches where nutrient scavenging is essential for survival and virulence (da Silva et al., 2002; Kim et al., 2016). The term "TonB-dependent receptor/Oar-like" likely refers to a subset of TBDRs with signaling functions, analogous to outer membrane transducers in other bacteria (e.g., TonB-dependent transducers that transmit signals across the envelope to regulate virulence genes) or proteins resembling Oar (outer membrane antibiotic resistance) or OryR-like regulators in *Xanthomonas* (Ferluga & Venturi, 2008; Koebnik, 2005). In *Xoo*, such proteins may integrate nutrient sensing with pathogenicity regulation.

Structural and Genomic Features of TBDRs in *Xanthomonas oryzae* pv. *oryzae*

Xanthomonas genomes, including PXO99^A, encode an exceptionally large repertoire of TBDRs (approximately 70–100), far exceeding most other bacteria, underscoring their adaptation to plant-associated, nutrient-poor niches (Salzberg et al., 2008). A subset of TBDRs exhibits signaling functions as TonB-dependent transducers (sometimes termed Oar-like proteins, referencing the outer membrane-associated regulator Oar in *Myxococcus* or analogous transducer families in *Xanthomonads*). These proteins sense external ligands and transmit signals across the envelope to regulate virulence gene expression (Koebnik, 2005). In PXO99^A and related strains, such transducer-like TBDRs may link nutrient availability to *hrp* regulon activation or quorum sensing. The fully sequenced genome of *Xoo* strain PXO99^A (4.94 Mbp) encodes nearly 79 putative TBDRs, similar to other sequenced *Xoo* strains (e.g., KACC10331 and MAFF311018) but with strain-specific variations, including unique insertions and effector complements. The strain PXO99^A TBDRs are organized in diverse loci, many clustered with carbohydrate utilization genes or iron acquisition operons, reflecting dual roles in siderophore and polysaccharide uptake (Salzberg et al., 2008). Structurally, PXO99^A TBDRs conform to the canonical architecture: a 22-stranded β -barrel with an N-terminal plug domain and a periplasmic TonB box for interaction with TonB (Schauer et al., 2008). The TonB-ExbB-ExbD system is conserved, with multiple exbD paralogs as in related *Xanthomonads*. Proteomic analyses of PXO99^A infected rice have identified multiple TBDRs as differentially accumulated proteins, with nine TBDRs showing reduced abundance in incompatible interactions (e.g., with resistant rice line H471), suggesting host suppression of bacterial nutrient uptake as a defence mechanism (Wang et al., 2020). Bioinformatic screening of the PXO99^A proteome (4,951 proteins) highlights forty eight TonB-dependent outer membrane receptors among secreted/enzymatic virulence factors, often co-predicted with Sec/SPI secretion signals and pathogenic annotations (Kashyap and Khan 2023; Kashyap et al., 2024).

Role in Iron Acquisition and Virulence

Iron is a limiting nutrient in the plant apoplast and xylem, where it is sequestered by host proteins. *Xoo* employs multiple iron uptake systems, including ferrous iron via FeoABC and ferric iron via siderophores. Mutational studies demonstrate that the FeoB ferrous transporter is essential for full virulence, with *feoB* mutants showing reduced lesion lengths on rice. For ferric iron, *Xoo* produces a vibrioferrin-like siderophore encoded by the *xss* operon (*xssA-E* for synthesis, *xsuA* as the TBDR for ferric-siderophore uptake). While *xss* mutants are siderophore-deficient but virulence-proficient (likely due to redundancy with Feo), the *xsuA* TBDR is specific for native siderophore utilization (Pandey & Sonti, 2010).

Role in Carbohydrate Scavenging and Adaptation to the Plant Environment

Phytopathogenic *Xanthomonas* exhibit expanded TBDR families for plant polysaccharide uptake, a feature shared with aquatic bacteria but rare in enteric ones. In *xcc*, CUT loci enable scavenging of xylan, pectin, and sucrose derivatives via dedicated TBDRs, with mutants impaired in epiphytic survival or lesion expansion. *Hrp* regulons in *Xanthomonas* include some TBDRs (e.g., in *Xcc*, *hrpG/X*-regulated TBDRs contribute weakly to pathogenicity), hinting at coordinated expression with T3SS during infection (Blanvillain et al., 2007).

TonB-Dependent Transducers and Oar-Like Signalling in Pathogenicity

Certain TBDRs function as transducers, sensing substrates and transducing signals via TonB to inner membrane regulators (Koebnik, 2005). In *X. axonopodis* pv. *citri*, a TonB-dependent transducer (XAC4131) regulates pathogenicity genes ((Aini et al., 2010)). The TBDRs are multifaceted virulence determinants in *Xoo*, enabling iron and carbohydrate acquisition in hostile plant environments and potentially transducing signals for pathogenicity gene regulation. Their expansion in *Xanthomonas* genomes reflects evolutionary adaptation to phyto-pathogenicity. While iron-focused TBDRs (e.g., *XsuA*) support growth, emerging evidence for carbohydrate-specific ones (e.g., *sux*) highlights exploitation of host resources (Sadoine et al., 2021). TonB-dependent outer membrane receptors and their transducer/Oar-like counterparts are critical virulence determinants, enabling iron and carbohydrate acquisition in the hostile xylem while potentially sensing cues to activate pathogenicity programs. Genomic expansion of TBDRs reflects evolutionary fine-tuning for rice infection. Proteomic evidence for rice interactions highlights host targeting of these systems during resistance. A subtractive genomic and proteomic approach has identified TonB-dependent receptors as potential antimicrobial targets due to their surface localization and essential roles in pathogenesis. Their outer membrane positioning makes them accessible to inhibitory molecules, their-by paving a way towards integrated disease management and the design of novel bactericidal compounds for rice blight control. With this motivation the team carried a computational work with vigorous methodology to model two receptors and screen a set of ZINC15 database ligands to inhibit their functionality

MATERIALS AND METHODS

1. Comprehensive Profiling of Virulence Factors: Sequence, Function, and Cellular Localization

A comprehensive genomic and proteomic analysis of *Xanthomonas oryzae* pv. *oryzae* strain PXO99^A, a major rice pathogen, was carried out using the ENTREZ platform of GenBank database. The analysis includes retrieving the organism's complete genome sequence along with its annotated genes and corresponding protein sequences (Salzberg et al., 2008). To identify potential virulence factors, the MP3 standalone software and MP4 server, both developed by the Indian Institute of Science Education and Research (IISER) Bhopal were employed. These specialized machine learning-based platforms utilize Support Vector Machines (SVMs) and Hidden Markov Models (HMMs) to achieve rapid, sensitive, and highly accurate detection of virulence-associated genes/proteins in microbial and metagenomic datasets (Gupta et al., 2017; Gupta et al., 2022). Given the importance of secreted proteins in host-pathogen interactions and immune system evasion, their identification was a key component of the study. SignalP 6.0, developed by the Technical University of Denmark, was used to predict protein secretion signals with high precision (Teufel et al., 2021). Subsequently, functional characterization of these proteins was performed using EzyPred server, a hierarchical classification tool that predicts enzymatic activity levels (0–2 according to the Enzyme Commission system) by integrating sequence data, domain features, and evolutionary information (Shen & Chou, 2007). Finally, the subcellular localization of the predicted proteins within the bacterial cell was determined using PSLpred, a prediction server specifically designed for Gram-negative bacteria. PSLpred combines PSI-BLAST alignment with SVM-based classification, incorporating dipeptide composition and physicochemical parameters to achieve over 91% prediction accuracy (Bhasin et al., 2005). Various other secondary property analysis of proteins done using Expasy sever. (Artimo et al., 2012)

2. Computational construction of protein architecture: Modelling, Validation, and Functional Annotation

The three-dimensional structures of Ton-B dependent receptors were predicted using the Google Colab-based implementation of AlphaFold2 (Guo et al., 2022), a deep learning platform renowned for its high accuracy in protein structure prediction (Mariani et al., 2013). For each enzyme sequence, the server generated five models. The top-ranking model, as determined by predicted confidence scores (pLDDT and pTM), was selected for further analysis. To optimize stereochemistry, the selected models underwent energy minimization using the YASARA Energy Minimization Server (Krieger et al., 2009; Krieger & Vriend, 2014). This process employs advanced force fields to relieve steric clashes and refine the geometry, resulting in stable, low-energy conformations. The structural validity and stereo-chemical quality of the refined models were rigorously assessed using a suite of bioinformatic tools accessible through the SAVES server:

1. ModFOLD9 (McGuffin et al., 2024) was used for global and local model quality estimation.
2. ERRAT (Colovos & Yeates, 1993) analysed the statistics of non-bonded atomic interactions.
3. VERIFY3D (Eisenberg et al., 1997; Lüthy et al., 1992) evaluated the compatibility of the amino acid sequence with its predicted 3D environment.
4. PROCHECK (Laskowski et al., 1993) and VADAR (Willard, 2003) were employed for in-depth stereo-chemical analysis, including the assessment of dihedral angles via Ramachandran plots (Lovell et al., 2003; Ramachandran et al., 1963).

3. Integrated Analysis of Ligand-Binding Cavities and Their Pharmacophoric Features

The identification and functional annotation of protein cavities were conducted with the Cavity-Plus platform (Xu et al., 2018; Wang et al., 2023). This resource leverages the CAVITY method to systematically locate and prioritize ligand-binding sites according to their steric and physicochemical suitability. For selected cavities, in-depth pharmacophore analysis was carried out using the platform's integrated Cav-Pharmer tool.

4. In Silico Screening of a Natural Products Using Library from ZINC15

ZINC15, a comprehensive database comprising commercially accessible small molecules, with access to over 750 million compounds for use in virtual screening and structure-based drug discovery. Within ZINC15, the Secondary Metabolite subset includes naturally derived compounds produced by various organisms. These molecules, having evolved to interact with biological systems, serve as promising candidates for modulating protein activity and influencing cellular processes. In the present study, a set of 80,617 ligands from this subset was selected for virtual screening against the computationally identified enzymatic targets (Sterling & Irwin, 2015).

The MTiOpenScreen server, a web-based platform that facilitates structure-based virtual screening, assisting in the identification of potential lead compounds targeting specific proteins. Utilizing the AutoDock Vina docking engine, the platform enables large-scale screening of small-molecule libraries and prediction of ligand-binding affinities. It provides an interactive interface for uploading protein structures, selecting ligand databases, and interpreting docking outcomes (Labbé et al., 2015).

DockThor server, another online molecular docking server designed to predict the binding conformations and affinities of small molecules toward target proteins. It employs a Lamarckian genetic algorithm to perform flexible ligand docking while accounting for both ligand dynamics and the structural properties of receptor binding sites. With its user-friendly submission system and integrated visualization tools, DockThor aids in evaluating binding interactions and identifying potential lead candidates (de Magalhães et al., 2004; Santos et al., 2020).

5. Evaluation of ligand molecular and ADMET properties

The AI Drug Lab at Southern Methodist University (SMU), directed by the Tao Research Group within the Department of Chemistry, is dedicated to the integration of artificial intelligence in drug discovery and design. The laboratory utilizes advanced machine learning and deep learning frameworks to enhance various stages of drug development and optimization. Its major research competencies include accurate ADMET property prediction using ensembles of molecular descriptors and tree-based

machine-learning algorithms; identification of protein allosteric sites through a combination of extreme gradient boosting and graph convolutional neural networks; accelerated exploration of protein conformational landscapes via latent space-assisted adaptive sampling; and evaluation of protein allostery using relative entropy-based dynamical allosteric network analysis across multiple structural hierarchies (Tian et al., 2022).

6. Binding Mode Analysis and Interaction Profiling

The prediction of ligand-binding poses was conducted through site directed docking simulations on the SwissDock platform (Grosdidier et al., 2011). This server utilizes the EADock DSS algorithm to identify potential binding sites and forecast interaction energies. For the visual analysis of molecular recognition, the protein-ligand complexes were subjected to interaction profiling using LigPlot+ software, which provides comprehensive 2D schematics of hydrogen bonding, hydrophobic contacts, and interactions with solvent molecules and metal ions (Laskowski & Swindells, 2011).

RESULTS AND DISCUSSION

1. Comprehensive Profiling of Virulence Factors: Sequence, Function, and Cellular Localization

The proteome of *Xanthomonas oryzae* pv. *oryzae* strain PXO99A was initially screened for virulence factors using the MP3 standalone tool. This analysis identified 738 proteins as virulent, with Support Vector Machine (SVM) scores ranging from 1.0015 to 7.206, indicating a high probability of involvement in pathogenicity. Subsequent functional classification via the MP4 server categorized these putative virulence factors, with 491 proteins predicted as Class 3 (e.g., secretory systems and capsular components for host invasion) and 235 as Class 2 (e.g., antibiotic resistance proteins and toxins). Secretory protein analysis using SignalP 6.0 predicted 134 proteins for secretion via the classical Sec/SPI pathway. From this subset, 14 secreted proteins were forecast by EzyPred to possess enzymatic functions critical for virulence.

These enzymes facilitate nutrient acquisition, host immune evasion, and antibiotic resistance, and include:

- A. Polysaccharide-degrading enzymes: Xylosidase, Arabinosidase, Exoglucanase, Endoglucanase, Cellulase, Xylanase, and Pectinesterase.
- B. Oxidative stress-related enzymes: Cytochrome C peroxidase and Superoxide dismutase.
- C. Antibiotic resistance enzyme: β -Lactamase.
- D. Other virulence-associated proteins: Lipase/Esterase, and Cytochrome biogenesis proteins.
- E. Iron uptake related proteins: TonB-dependent receptors

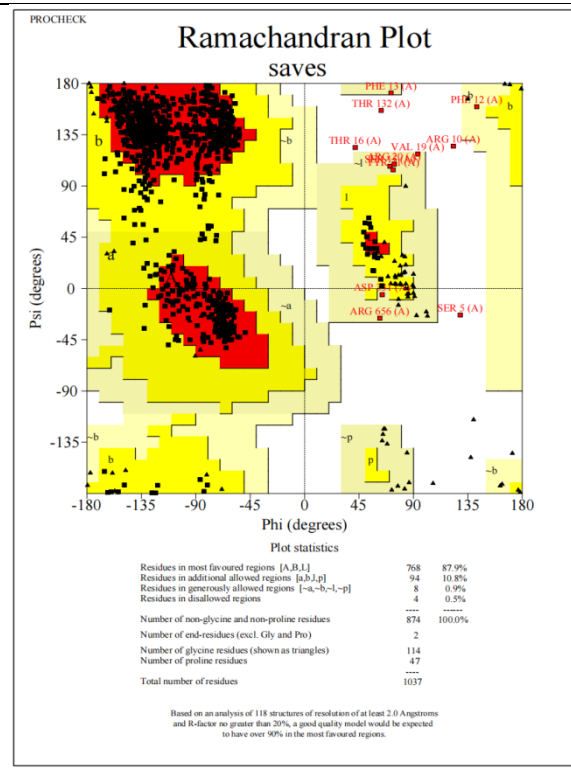
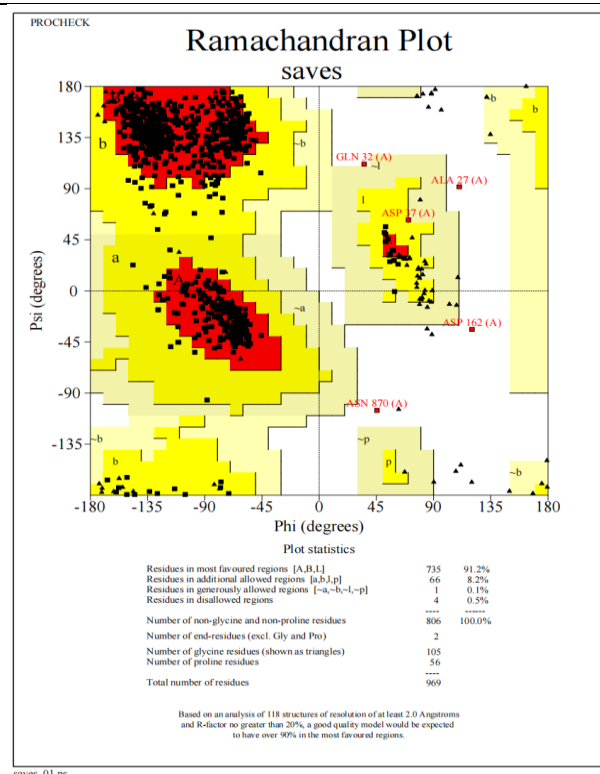
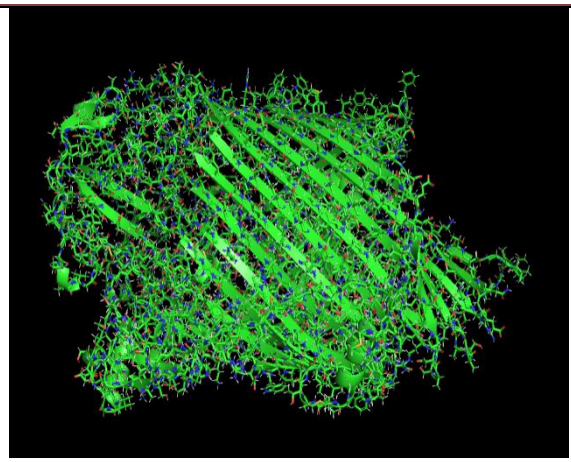
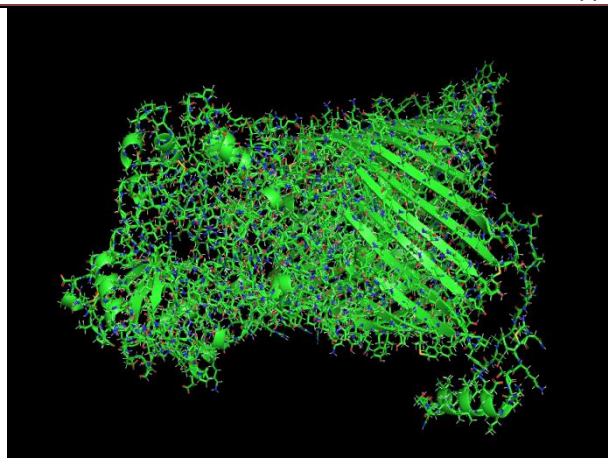
The Subcellular localization profiling with the PSLpred server provided further context for the potential function of these enzymes. The predictions indicated six extracellular enzymes (Exoglucanase, Endoglucanase, Pectinesterase, Lipase, Xylanase), two outer membrane proteins (TonB-dependent receptors), one inner membrane protein (Cytochrome biogenesis protein), and five periplasmic proteins (Xylosidase, Arabinosidase, Cytochrome C peroxidase, β -Lactamase, Cellulase, Superoxide dismutase).

2. Computational construction of protein architecture: Modelling, Validation, and Functional Annotation

Both TonB-dependent outer membrane receptor proteins were analysed. The first protein (ACD59730.1, TonB-dependent outer membrane receptor) is 969 amino acids long, while the second (ACD60174.1, TonB-dependent receptor/Oar-like receptor) is longer at 1037 amino acids. AlphaFold predictions for both models showed high confidence, with the first achieving a mean pLDDT of 91.6 and pTM score of 0.88, and the second a mean pLDDT of 90.1 and pTM score of 0.888; each model used 20 PDB templates (e.g., 2hdf_A, 3rgm_A, 3rgn_A, 1nqe_A, 3m8b_A for the first; 1fep_A, 6r1f_A, 6i2j_A, 5mzs_A, 5out_A for the second). Subsequent YASARA energy minimization substantially improved both structures, reducing energy by 8628.0 kcal/mol (from -496713.4 to -505341.4 kcal/mol) for ACD59730.1 and by 11479.6 kcal/mol (from -504266.8 to -515746.6 kcal/mol) for ACD60174.1. Model quality assessment further supported the reliability of both structures. ModFOLD reported very high confidence (CERT) for ACD59730.1 with a P-value of 1.23×10^{-4} and Global Model Quality Score of 0.8203. The ERRAT overall quality scores were 83.65% for the first protein and a higher 92.71% for the second. VERIFY3D passed 88.26% and 84.33% of residues (3D-1D score ≥ 0.1), respectively. VADAR estimated folding free energies of -805.86 (observed) and -943.29 kcal/mol (expected) for ACD59730.1 versus -860.87 and -1010.61 kcal/mol for ACD60174.1. Finally, PROCHECK Ramachandran analysis showed favorable stereochemistry for both: 87.7% core, 11.6% allowed, 0.5% generously allowed, and only 0.2% disallowed regions for the first protein, improving slightly to 87.9%/10.8%/0.9%/0.5% for the second; both models had excellent bond length/angle scores (4.3 and 4.4), no bad contacts, and >91% of planar groups within limits. Overall, both predicted structures exhibit high quality and are suitable for further structural and functional studies, with ACD60174.1 showing marginally better ERRAT and energy minimization outcomes despite comparable global confidence metrics. The table no. 1 provides a pictorial of results, while the table no. 2 provides a tabular representation.

Table no 1::Figures representing the modelled 3'D structure form Google Alpha-fold server, Ramachandran plot and Verify 3D server analysis for ACD59730.1 TonB-dependent outer membrane Receptor and ACD60174.1 TonB-dependent Receptor/Oar-like protein.

ACD59730.1 TonB-dependent outer membrane Receptor	ACD60174.1 TonB-dependent Receptor/Oar-like receptor
3'D modelled structure	3'D modelled structure



Verify 3D server result

Verify 3D server result

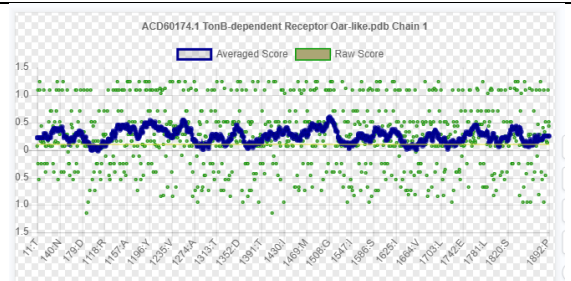
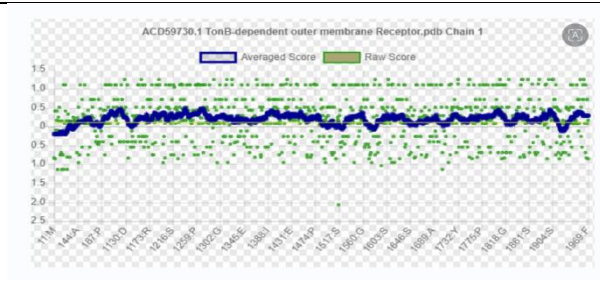


Table no 2::A tabular analysis of both proteins structure validation results using various parameters

Receptor	ACD59730.1; TonB-dependent outer membrane Receptor	ACD60174.1 TonB-dependent Receptor/Oar-like receptor
Amino Acid Length	969	1037
3D Structure Prediction	20 PDB templates (e.g., '2hdf_A', '3rgm_A', '3rgn_A', '1nqe_A',	20 PDB templates (e.g. 1fep_A', '6r1f_A', '6i2j_A', '5mzs_A', '5out_A',)

	'3m8b_A')	
pLDDT Score	91.6	90.1
pTM Score	0.88	0.888
YASARA Energy Minimization (kcal/mol)	Initial: -496713.4 Final: -505341.4 Reduction: 8628.0	Initial: -504266.8 Final: -515746.6 Reduction: 11480.6
ModFOLD Server (v9.0)	Confidence: CERT P-value: 1.23E-4 Global Model Quality Score: 0.8203	Confidence: NA P-value: NA Global Model Quality Score: NA
ERRAT Server Analysis (%)	Overall Quality: 83.654%	Overall Quality: 92.705
VERIFY3D Server Analysis	88.26% residues with 3D-1D score \geq 0.1	84.33% residues with 3D-1D score \geq 0.1
VADAR Server Analysis (Observed vs Expected Free Energy of folding in Kcal/mol)	-805.86 and -943.29	-860.87 and -1010.61
PROCHECK Server Analysis (Ramachandran Plot analysis)	Core: 87.7 % Allowed: 11.6% Generously-Allowed: 0.5% Disallowed: 0.2% Bond-Length/Angle-Score:4.3, Bad Contacts: 0, Planar groups: 91.6% within limits	Core: 87.9% Allowed: 10.8% Generously-Allowed: 0.9% Disallowed: 0.5% Bond Length/Angle Score: 4.4, Bad Contacts: 0, Planar groups: 92.4% within limits

3. Integrated Analysis of Ligand-Binding Cavities and Their Pharmacophoric Features

For receptor ACD59730, 25 cavities were detected in total. The most promising pocket exhibited a maximum predicted pKd of 7.17, an average pKd of 6.72, and a high Drug Score of 2282.00, classifying it as strongly druggable. This pocket presents a large surface area of 3339.25 Å² and a volume of 9180.62 Å³, with bounding box dimensions of 30.5 × 35.0 × 23.0 Å centred at (-14.25, 17.0, 18.5) Å. It is richly decorated with interaction centres, including 30 hydrogen-bond donors, 25 acceptors, 14 hydrophobic centres, and 10 negative electrostatic centres (no positive centres). The pocket is lined by six key residues: Thr59, Val63, Val719, Thr729, Asp825, and Gly806. In comparison, receptor ACD60174 showed an even higher-affinity predicted pocket with a maximum pKd of 7.28, average pKd of 6.73, and a markedly higher Drug Score of 6231.0, also classified as strongly druggable. This pocket is significantly larger, with a surface area of 8504.0 Å² and volume of 15593.88 Å³, enclosed in a box of dimensions 44.0 × 60.0 × 61.5 Å centred at (12.5, -0.5, -1.75) Å. It contains 63 hydrogen-bond donor centres, 31 acceptor centres, and 4 hydrophobic centres, but notably lacks both positive and negative electrostatic centres. The key interacting residues in this pocket are Asn192, Val421, Asn215, Gln449, Ile220, and Thr218. Both receptors possess large, strongly druggable cavities with high predicted ligand-binding affinity, making them attractive targets for structure-based drug design against these outer membrane proteins. The pocket in ACD60174 appears particularly spacious and shows superior Drug Score, while that in ACD59730 offers a more diverse set of polar and charged interaction features. A tabular comparison is available in table no 3.

Table no 3::A summary of cavity characterization and pharmacological profiling of proteins using Cavity-Plus server

Property And Receptor ID	Total Cavities	Predicted Maximum pKd	Average pKd	Drug Score	Druggability Type	Surface Area (Å ²)	Volume (Å ³)	Box Dimensions (X, Y, Z) in Å	Box Center (X, Y, Z) in Å	H-bond Donor Centers	H-bond Acceptor Centers	Hydrophobic Centers	Positive Electrostatic Centers	Negative Electrostatic Centers	Number of Residues	Key Residues
ACD59730	25	7.17	6.72	2282.00	Strong	3339.25	9180.62	30.5, 35.0, 23.0	-14.25, 17.0, 18.5	30	25	14	0	10		Thr59 Val63 Val719 Thr729 Asp825 Gly806
ACD60174	7.28	6.73	6.73	6231.0	Strong	8504.0	15593.88	44.0, 60.0, 61.5	12.5, -0.5, -1.75	63	31	4	0	0		Asn192 Val421 Asn215 Gln449 Ile220 Thr218

4. In Silico Screening of a Natural Products Using Library from ZINC15, Evaluation of ligand molecular and ADMET properties and Binding Mode Analysis and Interaction Profiling

ACD59730.1 TonB-dependent outer membrane Receptor

The MTIOpen Screen server was utilized for screening purpose. The DockThor VS server showed promising results for some selected ligands. The molecular docking results for the top three compounds are as follows. The highest-scoring ligand, with ID ZINC000022400820, achieved a binding score of -8.5 kcal/mol, with a total energy of 35.665 kcal/mol, internal energy of -37.67 kcal/mol, van der Waals energy of -28.946 kcal/mol, and electrostatic energy of -8.724 kcal/mol. The second-ranked compound, with ZINC000024841601, exhibited a binding score of -8.218 kcal/mol, accompanied by a total energy of 20.202 kcal/mol, internal energy of -36.02 kcal/mol, van der Waals contribution of -23.681 kcal/mol, and electrostatic energy of -12.339 kcal/mol. The third compound, with ID ZINC000014741520, showed a closely similar binding score of -8.208 kcal/mol, with a total energy of 73.347 kcal/mol, internal energy of -33.395 kcal/mol, van der Waals energy of -26.228 kcal/mol, and electrostatic energy of -7.167 kcal/mol. Three ligands were analyzed for their molecular properties toxicity and docking.

The ligand 1, exhibits favorable physicochemical properties with a molecular weight of 464.2 Da, nine heteroatoms, twelve rotatable bonds, and two rings, all classified as optimal. It contains six hydrogen-bond acceptors (HA) and one hydrogen-bond donor (HD), also within the optimal range, and a balanced lipophilicity reflected by a log KOW of 3.35. In terms of absorption, the predicted Caco-2 permeability is -5.16 log(cm/s), human intestinal absorption (HIA) is 70.86%, and P-glycoprotein inhibition probability is 40.23%, while log D at pH 7.4 is 1.79 and aqueous solubility is -3.85 log(mol/L), indicating moderate solubility. Oral bioavailability is predicted at 48.71%. Regarding toxicity, the probabilities of hERG channel blockade, Ames mutagenicity, and drug-induced liver injury (DILI) are 46.04%, 45.28%, and 48.49%, respectively, suggesting relatively low risk in each category, and the predicted acute oral toxicity (LD50) in rats is 2.19 -log(mol/kg), corresponding to moderate toxicity. Overall, the compound displays an optimal and drug-like profile with good absorption potential and acceptable safety margins. The ligand demonstrated strong docking affinities of -6.884, -6.569, and -6.375 Kcal/mol for three different poses.

The ligand 2, possesses highly drug-like physicochemical properties, with a molecular weight of 368.12 Da, six heteroatoms, five rotatable bonds, and three rings, all rated optimal. It features three hydrogen-bond acceptors and two hydrogen-bond donors, together with a favorable log KOW of 2.73, indicating balanced lipophilicity. Absorption predictions are promising, showing Caco-2 permeability of -5.54 log(cm/s), human intestinal absorption (HIA) of 72.33%, P-glycoprotein inhibition probability of 40.41%, log D7.4 of 1.9, and aqueous solubility of -4.39 log(mol/L), while oral bioavailability is estimated at 48.22%. Distribution characteristics are also favorable, with blood-brain barrier penetration probability of 30.27%, plasma protein binding rate (PPBR) of 47.8%, and a steady-state volume of distribution (VDss) of 3.2 L/kg. Toxicity profiles remain acceptable, with hERG blockade probability at 42.27%, Ames mutagenicity risk at 44.59%, drug-induced liver injury (DILI) likelihood at 54.71%, and predicted acute oral LD50 of 1.52 -log(mol/kg), corresponding to moderate toxicity. Overall, the compound demonstrates an excellent drug-like profile with good absorption, moderate distribution, and low-to-moderate safety concerns. The results showed docking affinities of -7.209, -7.205, and -7.157 Kcal/mol for three different poses.

The ligand no 3, displays a highly favorable drug-like profile with a molecular weight of 413.21 Da, nine heteroatoms, six rotatable bonds, and four aromatic/ring systems, all within optimal ranges. It contains seven hydrogen-bond acceptors and no hydrogen-bond donors, paired with a moderate log KOW of 0.75, reflecting balanced hydrophilicity-lipophilicity. Absorption predictions are strong, with Caco-2 permeability of -5.35 log(cm/s), human intestinal absorption (HIA) of 74.83%, low P-glycoprotein inhibition probability of 40.95%, log D7.4 of 1.63, and aqueous solubility of -4.5 log(mol/L); oral bioavailability is predicted at 43.31%. Distribution properties are excellent, showing blood-brain barrier penetration probability of 32.42%, plasma protein binding of 49.12%, and a volume of distribution at steady state (VDss) of 3.67 L/kg. Toxicity risks remain low to moderate, with hERG blockade probability at 48.1%, Ames mutagenicity risk at 45.75%, drug-induced liver injury (DILI) likelihood at 43.38%, and acute oral LD50 of 2.24 -log(mol/kg), indicating moderate toxicity. In summary, the compound exhibits an outstanding overall profile with excellent absorption and distribution characteristics and acceptable safety margins. The ligand demonstrated promising docking affinities of -7.205, -7.205 and -7.157 -kcal/mol for three different poses.

ACD60174.1 TonB-dependent Receptor/Oar-like receptor

The MTIOpen Screen server was utilized for screening purpose. The DockThor-VS server showed promising results for some selected ligands. The top three poses exhibited promising binding affinities. The molecular docking results against the ACD60174.1 TonB-dependent receptor (Oar-like) reveal significantly stronger binding affinities compared to previous targets. The top-ranked compound, ZINC000014746740 exhibited the highest docking score of -11.24 kcal/mol, with a total energy of 116.432 kcal/mol, internal energy of -44.072 kcal/mol, van der Waals energy of -11.639 kcal/mol, and a highly favorable electrostatic contribution of -32.433 kcal/mol, indicating strong polar interactions with the receptor. The second compound, ZINC000085593982 achieved a docking score of -10.552 kcal/mol, supported by a total energy of 347.931 kcal/mol, internal energy of -43.085 kcal/mol, dominant van der Waals interactions of -38.213 kcal/mol, and electrostatic energy of -4.872 kcal/mol. The third-ranked ligand, ZINC000085593977 recorded a score of -8.505 kcal/mol, with a total energy of 373.46 kcal/mol, internal energy of -42.021 kcal/mol, van der Waals energy of -24.384 kcal/mol, and electrostatic energy of -17.637 kcal/mol. These results suggest that this TonB-dependent receptor binding pocket accommodates ligands with exceptionally high affinity, particularly the lead compound showing a docking score more than 2.7 kcal/mol better than previously evaluated targets. Three ligands were analyzed for their molecular properties toxicity and docking.

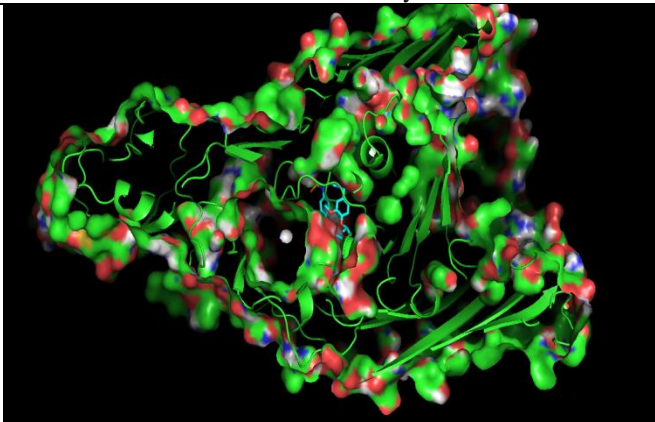
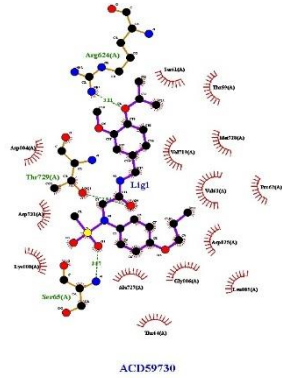
The ligand 1, presents a highly drug-like profile with a molecular weight of 487.26 Da, eight heteroatoms, seven rotatable bonds, and four rings, all within optimal limits. It possesses seven hydrogen-bond acceptors and one hydrogen-bond donor, along with

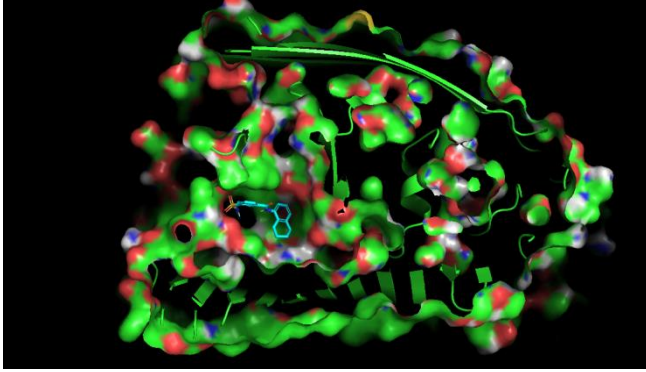
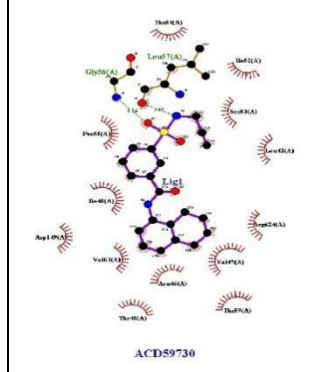
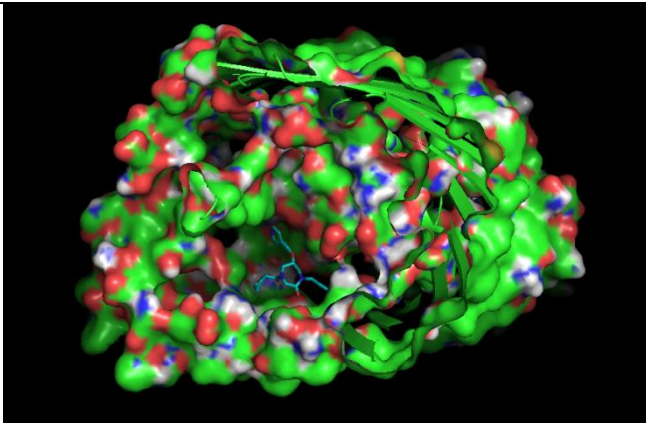
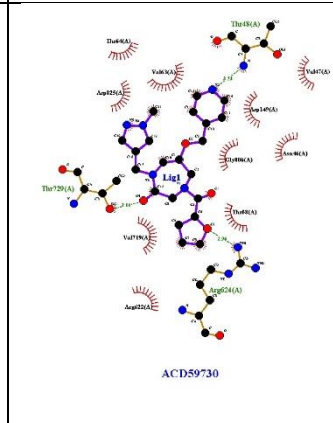
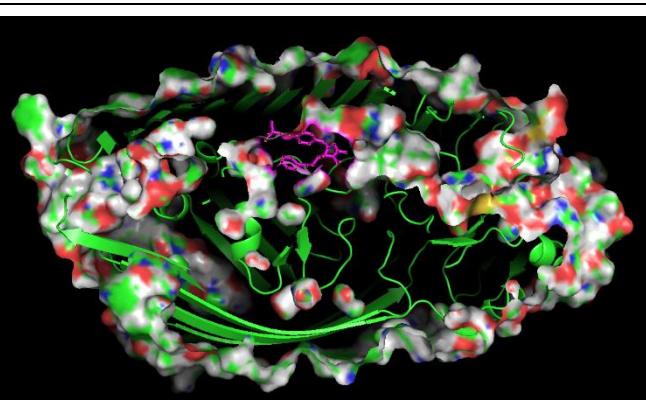
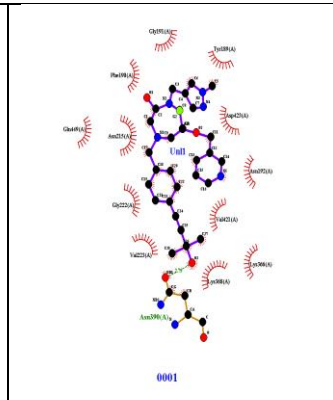
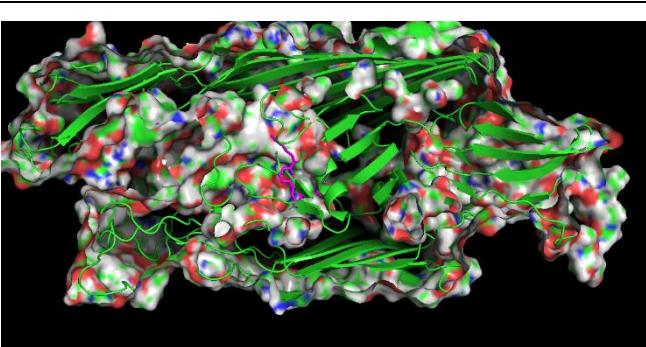
a well-balanced log KOW of 2.37. Absorption predictions are excellent, showing Caco-2 permeability of $-5.33 \log(\text{cm/s})$, human intestinal absorption (HIA) of 75.19%, log D7.4 of 1.87, and aqueous solubility of $-4.24 \log(\text{mol/L})$, with oral bioavailability estimated at 44.69%. Although P-glycoprotein inhibition probability is moderately elevated at 49.8%, it remains acceptable. Distribution properties are favorable, with blood-brain barrier penetration probability of 26.69%, plasma protein binding of 58.71%, and a steady-state volume of distribution (VD_{ss}) of 4.33 L/kg, suggesting good tissue distribution. Toxicity predictions for the compound indicate a generally acceptable safety profile. The probability of hERG channel blockade is 51.29%, representing a moderate cardiac risk that warrants further evaluation in vitro. Ames mutagenicity risk is low at 44.89%, suggesting negligible genotoxic potential. The likelihood of drug-induced liver injury (DILI) is 55.06%, which is slightly elevated but still within an acceptable range for continued development. Acute oral toxicity, expressed as predicted LD₅₀, is 2.08 $-\log(\text{mol/kg})$, corresponding to moderate toxicity comparable to many approved drugs. Overall, the compound exhibits no critical red flags in the predicted toxicity endpoints and appears suitable for follow-up studies. The ligand demonstrated strong docking affinities of -7.134 , -6.933 , and -6.786 Kcal/mol for three different poses.

The ligand 2, with a molecular weight of 682.34 Da, remains within the acceptable upper range for oral drug candidates and is classified as optimal. It contains eleven heteroatoms, nine rotatable bonds, seven rings, eleven hydrogen-bond acceptors, and three hydrogen-bond donors, all rated optimal despite pushing the boundaries of traditional Lipinski-type rules. The compound exhibits pronounced lipophilicity with a log KOW of 6.96, which is balanced by good predicted aqueous solubility of $-3.55 \log(\text{mol/L})$ and a log D7.4 of 2.01. Absorption characteristics are favorable, with Caco-2 permeability of $-5.27 \log(\text{cm/s})$, human intestinal absorption of 71.56%, low P-glycoprotein inhibition probability of 39.24%, and oral bio-availability of 34.85%, indicating reasonable though not exceptional oral exposure. Distribution is excellent, with a low blood-brain barrier penetration probability of 22.08%, moderate plasma protein binding of 53.12%, and a high volume of distribution of 4.94 L/kg, suggesting extensive tissue distribution. Toxicity predictions are acceptable, showing hERG blockade probability of 47.87%, Ames mutagenicity risk of 46.28%, DILI likelihood of 56.12%, and acute oral LD₅₀ of 2.38 $-\log(\text{mol/kg})$, corresponding to moderate toxicity. The results showed docking affinities of -7.758 , -7.648 , and -7.564 Kcal/mol .

The ligand 3, possessing a molecular weight of 612.26 Da, falls within the extended drug-like space and is rated optimal. It contains eleven heteroatoms, a low number of four rotatable bonds, seven rings, eleven hydrogen-bond acceptors, and three hydrogen-bond donors, all classified as optimal. Lipophilicity is moderately elevated with a log KOW of 4.94, yet remains balanced by favorable log D7.4 of 2.08 and predicted aqueous solubility of $-4.03 \log(\text{mol/L})$. Absorption predictions are strong, with Caco-2 permeability of $-5.29 \log(\text{cm/s})$, human intestinal absorption of 72.99%, low P-glycoprotein inhibition probability of 42.23%, and oral bioavailability of 39.78%, indicating viable oral absorption despite the compound's size. Distribution properties are highly favorable, featuring very low blood-brain barrier penetration (17%), moderate plasma protein binding of 39.34%, and a large volume of distribution of 5.08 L/kg, consistent with extensive tissue penetration. Toxicity endpoints are reassuringly low-to-moderate, with hERG blockade probability at 46.72%, Ames mutagenicity risk at 47.61%, drug-induced liver injury likelihood at 50.6%, and acute oral LD₅₀ of 2.36 $-\log(\text{mol/kg})$, reflecting moderate toxicity. Taken together, the compound exhibits a robust beyond-Rule-of-Five profile with excellent absorption, wide tissue distribution, minimal CNS exposure, and acceptable safety predictions, making it a promising candidate for further development. The ligand demonstrated promising docking affinities of -6.882 , -6.480 , and -6.438 kcal/mol . Table no 4 provides a pictorial representation of receptor-ligand interaction, table no 5 provides a tabular representation of receptor-ligand interaction and The Table no 6 provides a comparative tabular representation of receptor-ligand interaction

Table no 4 :: Pictorial representation of ligand interactions and LigPlot+ analysis.

ACD59730.1 TonB-dependent outer membrane Receptor interaction images with all three ligands along with LigPlot analysis		
Ligand 1 ZINC000022400 820		

<p>Ligand 2 ZINC000024841 601</p>		 <p>ACD59730</p>
<p>Ligand 3 ZINC000014741 520</p>		 <p>ACD59730</p>
<p>ACD60174.1 TonB-dependent Receptor/Oar-like receptor with all three ligands along with LigPlot analysis</p>		
<p>Ligand 1 ZINC000014746 740</p>		 <p>0001</p>
<p>Ligand 2 ZINC000085593 982</p>		

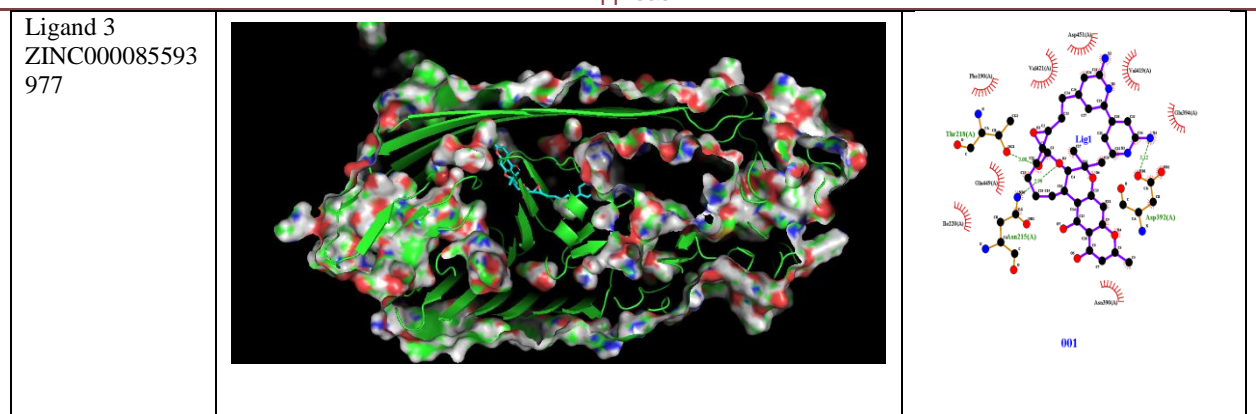


Table no 5. Ligands interactions with residues of enzyme using LigPlot+ analysis

<i>ACD59730.1 TonB-dependent outer membrane Receptor residues interaction with all three ligands</i>	
Ligand 1, ZINC000263585698	<i>Arg62, Ser61, Thr59, Met728, Val719, Val63, Pro60, Asp825, Leu805, Gly806, Ala727, Thr64, Ser65, Lys808, Asp731, Thr729, Asp804</i>
Ligand 2, ZINC000001087524	<i>Thr54, Ile52, Ser53, Leu42, Arg624, Val 47, Thr59, Asn 46, Thr48, Val63, Asp149, Ile45, Pro55, Gly56, Leu57</i>
Ligand 3, ZINC000002154369	<i>Thr48, Val47, Asp149, Gly806, Asn46, Thr48, Arg624, Arg622, Val719, Thr729, Asp825, Thr64, Val63</i>
<i>ACD60174.1 TonB-dependent Receptor/Oar-like receptor residues interaction with all three ligands</i>	
Ligand 1, ZINC000014746740	<i>Gly191, Tyr189, Asp423, Asn192, Val421, Lys366, Lys368, Asn350, Val223, Gly222, Asn215, Gln449, Phe150</i>
Ligand 2, ZINC000085593982	<i>Ile220, Gly221, Tyr206, Gly186, Val184, Gln185, Leu178, Glu174, Ala175, Ala170, Leu169, Ser172, Tyr1028, Arg171, Arg272, Gln1025, Asn192, Val201, Tle194, Asn219, Thr218</i>
Ligand 3, ZINC000085593977	<i>Asp45, Val415, Glu394, Asp392, Asn390, Asn215, Ile220, Gln449, Thr218, Phe190, Val421</i>

Table no 6 :: A summary table for various important ligands values as identified by Docking.

Receptors and Properties	ACD59730.1 TonB-dependent outer membrane Receptor			ACD60174.1 TonB-dependent Receptor/Oar-like receptor		
	Ligand 1 (Rank 1)	Ligand 2 (Rank 2)	Ligand 3 (Rank 3)	Ligand 1 (Rank 1)	Ligand 2 (Rank 2)	Ligand 3 (Rank 3)
ZINC ID	ZINC000014746740	ZINC000085593982	ZINC000085593977	ZINC000022400820	ZINC000024841601	ZINC000014741520
Docking Score vs ACD60174.1 (kcal/mol)	-11.24	-10.55	-8.51	-8.5	-8.218	-8.208
Total Energy (kcal/mol)	116.432	347.931	373.46	35.665	20.202	73.347
Internal Energy (kcal/mol)	-44.072	-43.085	-42.021	-37.67	-36.02	-33.395
van der Waals Energy (kcal/mol)	-11.639	-38.213	-24.384	-28.946	-23.681	-26.228
Electrostatic Energy (kcal/mol)	-32.433	-4.872	-17.637	-8.724	-12.339	-7.167
Additional docking scores (kcal/mol)	-7.134, -6.933, -6.786	-7.758, -7.648, -7.564	-6.882, -6.480, -6.438	-6.884, -6.569, -6.375	-7.209, -7.205, -7.157	-7.205, -7.205, -7.157
Molecular Weight (Da)	487.26	682.34	612.26	464.2	368.12	413.21

TonB-Dependent Receptors Activity Reduction Strategy in *Xanthomonas oryzae* pv. *oryzae* Pathogenicity: A Computational Approach

Number of Hetero-atoms	8	11	11	9	6	9
Number of Rotatable Bonds	7	9	4	12	5	6
Number of Rings	4	7	7	2	3	4
Hydrogen-bond Acceptors (HA)	7	11	11	6	3	7
Hydrogen-bond Donors (HD)	1	3	3	1	2	0
log KOW	2.37	6.96	4.94	3.35	2.73	0.75
Caco-2 Permeability (log cm/s)	-5.33	-5.27	-5.29	-5.16	-5.54	-5.35
Human Intestinal Absorption – HIA (%)	75.19	71.56	72.99	70.86	72.33	74.83
P-glycoprotein Inhibition (%)	49.8	39.24	42.23	40.23	40.41	40.95
Oral Bio-availability (%)	44.69	34.85	39.78	48.71	48.22	43.31
Blood-Brain Barrier Penetration – BBB (%)	26.69	22.08	17	26.69	30.27	32.42
Plasma Protein Binding Rate – PPBR (%)	58.71	53.12	39.34	58.1	47.8	49.12
hERG Blockade Probability (%)	51.29	47.87	46.72	46.04	42.27	48.1
Ames Mutagenicity Probability (%)	44.89	46.28	47.61	45.28	44.59	45.75
Drug-Induced Liver Injury – DILI (%)	55.06	56.12	50.6	48.49	54.71	43.38
Acute Oral Toxicity – LD50 (-log mol/kg)	2.08	2.38	2.36	2.19	1.52	2.24

SUMMARY AND CONCLUSION

A comprehensive in silico virulence factor screening of the *Xanthomonas oryzae* pv. *oryzae* strain PXO99A proteome identified 738 putative virulent proteins using the MP3 tool (SVM scores 1.00–7.21). Of these, 491 were classified as Class 3 (host invasion-related) and 235 as Class 2 (toxins and resistance proteins). SignalP 6.0 predicted 134 proteins to be secreted via the Sec/SPI pathway, and among them, EzyPred identified 14 secreted enzymes critical for pathogenicity. These enzymes include polysaccharide-degrading enzymes (xylosidase, arabinosidase, exoglucanase, endoglucanase, cellulase, xylanase, pectinesterase), oxidative stress protectors (cytochrome C peroxidase, superoxide dismutase), a β -lactamase, lipases/esterases, cytochrome biogenesis proteins, and notably two TonB-dependent outer membrane receptors involved in iron uptake. Subcellular localization (PSLpred) assigned six enzymes as extracellular, five as periplasmic, two as outer membrane (the TonB receptors), and one as inner membrane. High-confidence 3D structures of the two TonB-dependent receptors (ACD59730.1, 969 aa; ACD60174.1, 1037

aa) were generated using AlphaFold (mean pLDDT >90, pTM ≈0.88). The models were refined by YASARA energy minimization and rigorously validated by ModFOLD, ERRAT (>83%), VERIFY3D, VADAR, and PROCHECK (≤0.5% Ramachandran outliers), confirming excellent stereochemical quality suitable for downstream structural and drug-design studies. ACD60174.1 showed slightly superior ERRAT score and greater energy reduction upon minimization.

High-confidence 3D models were generated for both TonB-dependent outer membrane receptors from *Xanthomonas oryzae* pv. *oryzae* PXO99A using AlphaFold. ACD59730.1 (969 aa): mean pLDDT 91.6, pTM 0.88 while the ACD60174.1 (1037 aa, Oar-like): mean pLDDT 90.1, pTM 0.888. Both models were built from 20 high-quality PDB templates and further refined by YASARA energy minimization, achieving substantial stability gains (8,628 kcal/mol improvement for ACD59730.1 and 11,481 kcal/mol for ACD60174.1). Comprehensive validation confirmed excellent model quality like ModFOLD showed very high confidence (CERT, P-value 1.23×10^{-4} , GMQS 0.8203) for ACD59730.1. for ERRAT overall quality was 83.7% (ACD59730.1) vs. superior 92.7% (ACD60174.1). for VERIFY3D, values were 88.3% and 84.3% of residues passed, respectively. For VADAR folding free energy: both models showed highly favourable observed and expected values. For PROCHECK Ramachandran plot: both excellent, with ≥87.7% in core regions and only 0.2–0.5% disallowed residues; no bad contacts and high bond-length/angle scores (4.3–4.4)

Cavity detection and druggability prediction revealed large, highly druggable binding pockets in both receptors. For ACD59730.1, 25 cavities detected. The top pocket is classified as strongly druggable (max pKd 7.17, DrugScore 2282). It has a surface area of 3,339 Å² and volume of 9,181 Å³, rich in polar and charged features (30 H-bond donors, 25 acceptors, 14 hydrophobic, 10 negative centers; no positive centers). Key lining residues: Thr59, Val63, Val719, Thr729, Asp825, Gly806. For ACD60174.1, The best pocket is also strongly druggable but markedly superior (max pKd 7.28, outstanding DrugScore 6231). It is considerably larger (surface area 8,504 Å², volume 15,594 Å³) and predominantly polar/hydrophilic (63 H-bond donors, 31 acceptors, only 4 hydrophobic centers, no charged centers). Key residues: Asn192, Val421, Asn215, Gln449, Ile220, Thr218.

Virtual screening using the MTIOpen Screen platform followed by precise molecular docking on the DockThor-VS server identified promising small-molecule inhibitors for both TonB-dependent outer membrane receptors of *Xanthomonas oryzae* pv. *oryzae*. For receptor ACD59730.1, the top three hits displayed moderate but solid binding affinities of −8.5 kcal/mol (ZINC000022400820), −8.2 kcal/mol (ZINC000024841601), and −8.2 kcal/mol (ZINC000014741520). All three compounds are fully Lipinski-compliant (molecular weight 368–464 Da), exhibit good predicted oral absorption (human intestinal absorption 71–75%), moderate aqueous solubility, and low-to-moderate toxicity risks across hERG blockade, Ames mutagenicity, and drug-induced liver injury (probabilities ~40–55%), with rat acute oral LD50 values indicating only moderate toxicity. These molecules therefore safe, classically drug-like scaffolds ideal for subsequent hit-to-lead optimization. In striking contrast, the Oar-like receptor ACD60174.1 proved markedly more ligand-friendly, yielding dramatically stronger predicted binding affinities. The best compound (ZINC000014746740) achieved an outstanding docking score of −11.24 kcal/mol—more than 2.7 kcal/mol superior to the top hit on ACD59730.1—followed closely by −10.55 kcal/mol (ZINC000085593982) and −8.51 kcal/mol (ZINC000085593977). Although these ligands are larger (molecular weight 487–682 Da, extending beyond the classical Rule-of-5), they remain within acceptable extended drug-like space, retain favorable oral absorption, show excellent tissue distribution (VD_{ss} 4.3–5.1 L/kg), minimal CNS penetration, and toxicity profiles comparable to many approved antibacterials (hERG ~47–51%, DILI ~50–56%, moderate acute toxicity).

In conclusion, this study identifies a panel of secreted virulence-associated enzymes and, most prominently, two TonB-dependent outer membrane receptors from *Xanthomonas oryzae* pv. *oryzae* as highly promising targets for the development of novel anti-virulence strategies against bacterial leaf blight of rice. Both receptors (ACD59730.1 and the Oar-like ACD60174.1) were modeled with excellent accuracy using AlphaFold, refined by energy minimization, and rigorously validated, yielding high-confidence 3D structures fully suitable for structure-based drug design. ACD60174.1 consistently outperformed ACD59730.1 in several key metrics: superior local model quality (ERRAT 92.7%), greater energetic stabilization upon refinement, a markedly larger and more druggable binding pocket (Drug-Score 6231 vs. 2282), and dramatically stronger predicted ligand affinities in virtual screening and docking (best hit −11.24 kcal/mol vs. −8.5 kcal/mol). Consequently, while both receptors are demonstrably druggable and harbour deep cavities amenable to small-molecule inhibition, among both receptors the ACD60174.1 emerges as the clearly superior priority target. Its top-ranking ligands, although larger than classical Lipinski space, retain favourable ADME profiles, wide tissue distribution, low CNS penetration, and acceptable predicted safety, making them outstanding starting points for hit-to-lead optimization. The more conventional, weaker-binding series identified against ACD59730.1 provides a valuable backup chemo type.

Abbreviation

aa	amino acids
ADME	Absorption, Distribution, Metabolism, Excretion
CERT	Certainty (ModFOLD confidence level)
CNS	Central Nervous System
DILI	Drug-Induced Liver Injury
GMQS	Global Model Quality Score
H-bond	Hydrogen bond
hERG	human Ether-à-go-go-Related Gene (potassium channel)
HIA	Human Intestinal Absorption
LD50	Lethal Dose 50%

PDB	Protein Data Bank
pKd	negative logarithm of dissociation constant
pLDDT	predicted Local Distance Difference Test
pTM	predicted Template Modeling score
pv.	pathovar
Sec/SPI	Sec/Signal Peptidase I pathway
SVM	Support Vector Machine
VDss	Volume of Distribution at steady state
Xoo	<i>Xanthomonas oryzae</i> pv. <i>oryzae</i>
Å ²	square Ångström
Å ³	cubic Ångström

Acknowledgment

The authors thank the Dept. of Microbiology and Bioinformatics, Atal Bihari Vajpayee Vishwavidyalaya, Bilaspur, Chhattisgarh, India and Amity Institute of Biotechnology, Amity University Chhattisgarh, Raipur, Chhattisgarh, India for providing all the necessary infrastructure to carry-out the research work.

Conflict of Interest

No conflict of interest exists.

BIBLIOGRAPHY

1. Aini, L. Q., Hirata, H., & Tsuyumu, S. (2010). A TonB-dependent transducer is responsible for regulation of pathogenicity-related genes in *Xanthomonas axonopodis* pv. *citri*. *Journal of General Plant Pathology*, 76(2), 132–142. <https://doi.org/10.1007/s10327-010-0227-4>
2. Artimo, P., Jonnalagedda, M., Arnold, K., Baratin, D., Csardi, G., de Castro, E., Duvaud, S., Flegel, V., Fortier, A., Gasteiger, E., Grosdidier, A., Hernandez, C., Ioannidis, V., Kuznetsov, D., Liechti, R., Moretti, S., Mostaguir, K., Redaschi, N., Rossier, G., ... Stockinger, H. (2012). ExPASy: SIB bioinformatics resource portal. *Nucleic Acids Research*, 40(W1), W597–W603. <https://doi.org/10.1093/nar/gks400>
3. Bhasin, M., Garg, A., & Raghava, G. P. S. (2005). PSLpred: Prediction of subcellular localization of bacterial proteins. *Bioinformatics*, 21(10), 2522–2524. <https://doi.org/10.1093/bioinformatics/bti309>
4. Blanvillain, S., Meyer, D., Boulanger, A., Lautier, M., Guynet, C., Denancé, N., Vasse, J., Lauber, E., Arlat, M., & Redfield, R. J. (2007). Plant carbohydrate scavenging through TonB-dependent receptors: A feature shared by phytopathogenic and aquatic bacteria. *PLoS ONE*, 2(3), Article e224. <https://doi.org/10.1371/journal.pone.0000224>
5. Choi, Y., Kim, N., Mannaa, M., Kim, H., Park, J., Jung, H., Han, G., Lee, H., & Seo, Y. (2020). Characterization of Type VI secretion system in *Xanthomonas oryzae* pv. *oryzae* and its role in virulence to rice. *The Plant Pathology Journal*, 36(3), 289–296. <https://doi.org/10.5423/ppj.nt.02.2020.0026>
6. Colovos, C., & Yeates, T. O. (1993). Verification of protein structures: Patterns of nonbonded atomic interactions. *Protein Science*, 2(9), 1511–1519. <https://doi.org/10.1002/pro.5560020916>
7. Da Silva, A. C. R., Ferro, J. A., Reinach, F. C., Farah, C. S., Furlan, L. R., Quaggio, R. B., Monteiro-Vitorello, C. B., Van Sluys, M. A., Almeida, N. F., Alves, L. M. C., Amaral, A. M. D., Bertolini, M. C., Camargo, L. E. A., Camarotte, G., Cannavan, F., Cardozo, J., Chambergo, F., Ciapina, L. P., Cicarelli, R. M. B., ... Kitajima, J. P. (2002). Comparison of the genomes of two *Xanthomonas* pathogens with differing host specificities. *Nature*, 417(6887), 459–463. <https://doi.org/10.1038/417459a>
8. De Magalhães, C. S., Barbosa, H. J., & Dardenne, L. E. (2004). A genetic algorithm for the ligand-protein docking problem. *Genetics and Molecular Biology*, 27(4), 605–610. <https://doi.org/10.1590/s1415-47572004000400022>
9. Eisenberg, D., Lüthy, R., & Bowie, J. U. (1997). VERIFY3D: Assessment of protein models with three-dimensional profiles. *Methods in Enzymology*, 277, 396–404. [https://doi.org/10.1016/s0076-6879\(97\)77022-8](https://doi.org/10.1016/s0076-6879(97)77022-8)
10. Ferluga, S., & Venturi, V. (2008). OryR is a LuxR-family protein involved in interkingdom signaling between pathogenic *Xanthomonas oryzae* pv. *oryzae* and rice. *Journal of Bacteriology*, 190(6), 2292–2293. <https://doi.org/10.1128/JB.01672-07>
11. Grosdidier, A., Zoete, V., & Michielin, O. (2011). SwissDock, a protein-small molecule docking web service based on EADock DSS. *Nucleic Acids Research*, 39(Web Server issue), W270–W277. <https://doi.org/10.1093/nar/gkr366>
12. Guo, H., Perminov, A., Bekele, S., Kedziora, G., Farajollahi, S., Varaljay, V., Hinkle, K., Molinero, V., Meister, K., Hung, C., Dennis, P., Kelley-Loughnane, N., & Berry, R. (2022). AlphaFold2 models indicate that protein sequence determines both structure and dynamics. *Scientific Reports*, 12(1), Article 10665. <https://doi.org/10.1038/s41598-022-14382-9>
13. Gupta, A., Kapil, R., Dhakan, D. B., & Sharma, V. K. (2014). MP3: A software tool for the prediction of pathogenic proteins in genomic and metagenomic data. *PLoS ONE*, 9(4), Article e93907. <https://doi.org/10.1371/journal.pone.0093907>
14. Gupta, A., Malwe, A. S., Srivastava, G. N., Thoudam, P., Hibare, K., & Sharma, V. K. (2022). MP4: A machine-learning based classification tool for prediction and functional annotation of pathogenic proteins from metagenomic and genomic datasets. *BMC Bioinformatics*, 23(1), Article 546. <https://doi.org/10.1186/s12859-022-05061-7>
15. Kashyap, D., & Khan, A. (2023). In-silico subcellular localization and functional analysis of computationally predicted virulent proteins in *X. oryzae* pv. *oryzae* strain PXO99A causal organism of bacterial leaf blight (BLB) of rice (*O. sativa* L.). *Molecular Biology: Open Access*, 12(3), Article 377. <https://doi.org/10.37421/2168-9547.2023.12.377>

16. Kashyap, D., Shakya, A., & Kaladhar, D. (2024). Computational approaches in identification of virulent, secreted and enzymatic proteins type Sec/SPI of *Xanthomonas oryzae* pv. *oryzae* strain PXO99A pathogen of bacterial leaf blight disease in rice. *African Journal of Biomedical Research*, 27(1), 2450–2455. <https://doi.org/10.53555/ajbr.v27i1s.1827>
17. Kim, S., Cho, Y., Song, E., Lee, S. H., Kim, J., & Kang, L. (2016). Time-resolved pathogenic gene expression analysis of the plant pathogen *Xanthomonas oryzae* pv. *oryzae*. *BMC Genomics*, 17(1), Article 345. <https://doi.org/10.1186/s12864-016-2657-7>
18. Koebnik, R. (2005). TonB-dependent trans-envelope signalling: The exception or the rule? *Trends in Microbiology*, 13(8), 343–347. <https://doi.org/10.1016/j.tim.2005.06.005>
19. Krieger, E., Joo, K., Lee, J., Lee, J., Raman, S., Thompson, J., Tyka, M., Baker, D., & Karplus, K. (2009). Improving physical realism, stereochemistry, and side-chain accuracy in homology modelling: Four approaches that performed well in CASP8. *Proteins: Structure, Function, and Bioinformatics*, 77(Suppl. 9), 114–122. <https://doi.org/10.1002/prot.22570>
20. Krieger, E., & Vriend, G. (2014). YASARA View—molecular graphics for all devices—from smartphones to workstations. *Bioinformatics*, 30(20), 2981–2982. <https://doi.org/10.1093/bioinformatics/btu426>
21. Labbé, C. M., Rey, J., Lagorce, D., Vavruša, M., Becot, J., Sperandio, O., Villoutreix, B. O., Tufféry, P., & Miteva, M. A. (2015). MTiOpenScreen: A web server for structure-based virtual screening. *Nucleic Acids Research*, 43(W1), W448–W454. <https://doi.org/10.1093/nar/gkv306>
22. Laskowski, R. A., MacArthur, M. W., Moss, D. S., & Thornton, J. M. (1993). PROCHECK: A program to check the stereochemical quality of protein structures. *Journal of Applied Crystallography*, 26(2), 283–291. <https://doi.org/10.1107/s0021889892009944>
23. Laskowski, R. A., & Swindells, M. B. (2011). LigPlot+: Multiple ligand–protein interaction diagrams for drug discovery. *Journal of Chemical Information and Modeling*, 51(10), 2778–2786. <https://doi.org/10.1021/ci200227u>
24. Mariani, V., Biasini, M., Barbato, A., & Schwede, T. (2013). IDDT: A local superposition-free score for comparing protein structures and models using distance difference tests. *Bioinformatics*, 29(21), 2722–2728. <https://doi.org/10.1093/bioinformatics/btt473>
25. McGuffin, L. J., & Alharbi, S. M. A. (2024). ModFOLD9: A web server for independent estimates of 3D protein model quality. *Journal of Molecular Biology*, 436(7), Article 168531. <https://doi.org/10.1016/j.jmb.2024.168531>
26. Niño-Liu, D. O., Ronald, P. C., & Bogdanove, A. J. (2006). *Xanthomonas oryzae* pathovars: Model pathogens of a model crop. *Molecular Plant Pathology*, 7(5), 303–324. <https://doi.org/10.1111/j.1364-3703.2006.00344.x>
27. Noinaj, N., Guillier, M., Barnard, T. J., & Buchanan, S. K. (2010). TonB-dependent transporters: Regulation, structure, and function. *Annual Review of Microbiology*, 64(1), 43–60. <https://doi.org/10.1146/annurev.micro.112408.134247>
28. Pandey, A., & Sonti, R. V. (2010). Role of the FeoB protein and siderophore in promoting virulence of *Xanthomonas oryzae* pv. *oryzae* on rice. *Journal of Bacteriology*, 192(12), 3187–3203. <https://doi.org/10.1128/JB.01549-09>
29. Sadoine, M., Long, J., Song, C., Arra, Y., Frommer, W. B., & Yang, B. (2021). WITHDRAWN: Sucrose-dependence of sugar uptake, quorum sensing and virulence of the rice blight pathogen *Xanthomonas oryzae* pv. *oryzae*. *bioRxiv*. <https://doi.org/10.1101/2021.08.22.457195>
30. Salzberg, S. L., Sommer, D. D., Schatz, M. C., Phillippy, A. M., Rabinowicz, P. D., Tsuge, S., ... Bogdanove, A. J. (2008). Genome sequence and rapid evolution of the rice pathogen *Xanthomonas oryzae* pv. *oryzae* PXO99A. *BMC Genomics*, 9, Article 204. <https://doi.org/10.1186/1471-2164-9-204>
31. Santos, K. B., Guedes, I. A., Karl, A. L. M., & Dardenne, L. E. (2020). Highly flexible ligand docking: Benchmarking of the DockThor program on the LEADS-PEP protein-peptide data set. *Journal of Chemical Information and Modeling*, 60(2), 667–683. <https://doi.org/10.1021/acs.jcim.9b00905>
32. Schauer, K., Rodionov, D. A., & De Reuse, H. (2008). New substrates for TonB-dependent transport: Do we only see the ‘tip of the iceberg’? *Trends in Biochemical Sciences*, 33(7), 330–338. <https://doi.org/10.1016/j.tibs.2008.04.012>
33. Shen, H. B., & Chou, K. C. (2007). EzyPred: A top-down approach for predicting enzyme functional classes and subclasses. *Biochemical and Biophysical Research Communications*, 364(1), 53–59. <https://doi.org/10.1016/j.bbrc.2007.09.098>
34. Sterling, T., & Irwin, J. J. (2015). ZINC 15 – Ligand discovery for everyone. *Journal of Chemical Information and Modeling*, 55(11), 2324–2337. <https://doi.org/10.1021/acs.jcim.5b00559>
35. Teufel, F., Almagro Armenteros, J. J., Johansen, A. R., Gíslason, M. H., Pihl, S. I., Tsirigos, K. D., Winther, O., Brunak, S., von Heijne, G., & Nielsen, H. (2022). SignalP 6.0 predicts all five types of signal peptides using protein language models. *Nature Biotechnology*, 40(7), 1023–1025. <https://doi.org/10.1038/s41587-021-01156-3>
36. Tian, H., Ketkar, R., & Tao, P. (2022). ADMETboost: A web server for accurate ADMET prediction. *Journal of Molecular Modeling*, 28(12), Article 408. <https://doi.org/10.1007/s00894-022-05373-8>
37. Wang, L., Rong, W., & He, C. (2020). Comparative proteomic analysis reveals novel insights into the interaction between rice and *Xanthomonas oryzae* pv. *oryzae*. *Plants*, 9(8), Article 977. <https://doi.org/10.3390/plants9080977>
38. Wang, S., Xie, J., Pei, J., & Lai, L. (2023). CavityPlus 2022 update: An integrated platform for comprehensive protein cavity detection and property analyses with user-friendly tools and cavity databases. *Journal of Molecular Biology*, 435(14), Article 168141. <https://doi.org/10.1016/j.jmb.2023.168141>
39. Willard, L., Ranjan, A., Zhang, H., Monzavi, H., Boyko, R. F., Sykes, B. D., & Wishart, D. S. (2003). VADAR: A web server for quantitative evaluation of protein structure quality. *Nucleic Acids Research*, 31(13), 3316–3319. <https://doi.org/10.1093/nar/gkg565>
40. Xu, Y., Wang, S., Hu, Q., Gao, S., Ma, X., Zhang, W., Shen, Y., Chen, F., Lai, L., & Pei, J. (2018). CavityPlus: A web server for protein cavity detection with pharmacophore modelling, allosteric site identification and covalent ligand binding ability prediction. *Nucleic Acids Research*, 46(W1), W374–W379. <https://doi.org/10.1093/nar/gky380>